View metadata, citation and similar papers at core.ac.uk
brought to you by CORE
provided by Caltech Authors - Main

A real-time photoacoustic tomography system for small animals

John Gamelin,[1] Anastasios Maurudis[1], Andres Aguirre[1], Fei Huang[1], Puyun Guo[1], Lihong V. Wang[2], and Quing Zhu[1,*]

[1]*Department of Electrical Engineering, University of Connecticut, Storrs, CT 06269, USA*
[2]*Department of Biomedical Engineering, Washington University in St. Louis, St. Louis, MO 63130, USA*
zhu@engr.uconn.edu

Abstract: A real-time 512-element photoacoustic tomography system for small animal imaging using a ring ultrasound array has been developed. The system, based upon a 5 MHz transducer array formed along a 50 mm circular aperture, achieves sub-200 micron lateral resolution over a 2 cm disk-shaped region. Corresponding elevation resolutions of 0.6 to 2.5 mm over the central volume enable depth-resolved 3D tomographic imaging with linear translation. Using 8:1 electronic multiplexing, imaging at up to 8 frame/sec is demonstrated for both dynamic phantoms and *in vivo* mouse and brain samples. The real-time, full 2D tomographic capability of the system paves the way for functional photoacoustic tomographic imaging studies in small animals with sub-second time frame.

©2009 Optical Society of America

OCIS codes: (110.0110) Imaging Systems; (170.0170) Medical Optics and Biotechnology; (110.5120) Photoacoustic Imaging; (170.3880) Medical and Biological Imaging; (170.3890) Medical Optics Instrumentation; (170.6960) Tomography.

References and links

1. J. T. Oh, M. L. Li, H. F. Zhang, K. Maslov, G. Stoica, and L. V. Wang, "Three-dimensional imaging of skin melanoma *in vivo* by dual-wavelength photoacoustic microscopy," J. Biomed. Opt. **11**(3), 34032 (2006).
2. R. J. Zemp, R. Bitton, M. L. Li, K. K. Shung, G. Stoica, and L. V. Wang, "Photoacoustic imaging of the microvasculature with a high-frequency ultrasound array transducer," J. Biomed. Opt. **12**(1), 010501 (2007).
3. X. Wang, D. L. Chamberland, and D. A. Jamadar, "Noninvasive photoacoustic tomography of human peripheral joints toward diagnosis of inflammatory arthritis," Opt. Lett. **32**(20), 3002–3004 (2007).
4. G. F. Lungu, M. L. Li, X. Xie, L. V. Wang, and G. Stoica, "*In vivo* imaging and characterization of hypoxia-induced neovascularization and tumor invasion," Int. J. Oncol. **30**(1), 45–54 (2007).
5. E. Zhang, J. Laufer, and P. Beard, "Three-dimensional photoacoustic imaging of vascular anatomy in small animals using an optical detection system," Proc. SPIE **6437**, 64370S (2007).
6. S. Manohar, A. Kharine, J. C. van Hespen, W. Steenbergen, and T. G. van Leeuwen, "The Twente Photoacoustic Mammoscope: system overview and performance," Phys. Med. Biol. **50**(11), 2543–2557 (2005).
7. S. A. Ermilov, R. Gharieb, A. Conjusteau, and A. A. Oraevsky, "Hybrid optoacoustic and ultrasonic imaging system for detection of prostate malignancies," Proc. SPIE **6856**, 68560T (2008).
8. R. G. Kolkman, P. J. Brands, W. Steenbergen, and T. G. van Leeuwen, "Real-time *in vivo* photoacoustic and ultrasound imaging," J. Biomed. Opt. **13**(5), 050510 (2008).
9. J. J. Niederhauser, M. Jaeger, R. Lemor, P. Weber, and M. Frenz, "Combined ultrasound and optoacoustic system for real-time high-contrast vascular imaging *in vivo*," IEEE Trans. Med. Imaging **24**(4), 436–440 (2005).
10. S. Park, S. Mallidi, A. Karpiouk, S. Alyamov, and S. Emelianov, "Photoacoustic imaging using array transducer," Proc. SPIE **6437**, 643714 (2007).
11. B. Yin, D. Xing, Y. Wang, Y. Zeng, Y. Tan, and Q. Chen, "Fast photoacoustic imaging system based on 320-element linear transducer array," Phys. Med. Biol. **49**(7), 1339–1346 (2004).
12. Y. Lao, D. Xing, S. Yang, and L. Xiang, "Noninvasive photoacoustic imaging of the developing vasculature during early tumor growth," Phys. Med. Biol. **53**(15), 4203–4212 (2008).
13. S. Yang, D. Xing, Q. Zhou, L. Xiang, and Y. Lao, "Functional imaging of cerebrovascular activities in small animals using high-resolution photoacoustic tomography," Med. Phys. **34**(8), 3294–3301 (2007).
14. E. Z. Zhang, J. G. Laufer, R. B. Pedley, and P. C. Beard, "*In vivo* high-resolution 3D photoacoustic imaging of superficial vascular anatomy," Phys. Med. Biol. **54**(4), 1035–1046 (2009).
15. J. Gamelin, A. Aguirre, A. Maurudis, F. Huang, D. Castillo, L. V. Wang, and Q. Zhu, "Curved array photoacoustic tomographic system for small animal imaging," J. Biomed. Opt. **13**(2), 024007 (2008).

#109657 - $15.00 USD Received 3 Apr 2009; revised 17 May 2009; accepted 18 May 2009; published 8 Jun 2009
(C) 2009 OSA

16. J. Gamelin, A. Maurudis, A. Aguirre, F. Huang, P. Guo, L. H. V. Wang, and Q. Zhu, "A fast 512-element ring array photoacoustic imaging system for small animals," Proc. SPIE **7177**, 70 (2009).
17. J. A. Jensen, "Field: A Program for Simulating Ultrasound Systems," Med. Biol. Eng. Comput. **34**, 351–353 (1996).
18. J. Gamelin, A. Aguire, A. Maurudis, F. Huang, D. Castillo, L. H. V. Wang, and Q. Zhu, *Photoacoustic Imaging and Spectroscopy* (Taylor and Francis, 2008), Chap. 25.
19. M. Xu, and L. V. Wang, "Universal back-projection algorithm for photoacoustic computed tomography," Phys. Rev. E Stat. Nonlin. Soft Matter Phys. **71**(1 Pt 2), 016706 (2005).
20. M. Xu, and L. V. Wang, "Analytic explanation of spatial resolution related to bandwidth and detector aperture size in thermoacoustic or photoacoustic reconstruction," Phys. Rev. E Stat. Nonlin. Soft Matter Phys. **67**(5 Pt 2), 056605 (2003).
21. J. Gamelin, A. Maurudis, A. Aguirre, L. H. V. Wang, and Q. Zhu, "Improvements in time resolution of Tomographic Photoacoustic Imaging using a priori Information for Multiplexed Systems," Proc. SPIE **7177**, 49 (2009).
22. X. Wang, Y. Pang, G. Ku, X. Xie, G. Stoica, and L. V. Wang, "Noninvasive laser-induced photoacoustic tomography for structural and functional *in vivo* imaging of the brain," Nat. Biotechnol. **21**(7), 803–806 (2003).
23. X. Wang, G. Ku, M. A. Wegiel, D. J. Bornhop, G. Stoica, and L. V. Wang, "Noninvasive photoacoustic angiography of animal brains *in vivo* with near-infrared light and an optical contrast agent," Opt. Lett. **29**(7), 730–732 (2004).
24. X. Yang, L. V. Wang, A. Maurudis, J. Gamelin, and A. Aguirre, "Three-dimensional photoacoustic tomography of small animal brain with a curved array transducer," Proc. SPIE **7177**, 118–122 (2009).

1. Introduction

In recent years, biomedical photoacoustic imaging has demonstrated great potential for investigation of skin disorders [1,2], rheumatoid arthritis [3], brain vasculature [4,5], and cancerous lesions in the breast [6] and prostate [7]. The reliance upon ultrasonic signals for image formation not only confers a high penetration capability of up to 3 cm, but also enables the use of commercial ultrasound detection technologies for achieving real-time functional imaging. Many dynamic functional and *in vivo* studies require acquisition rates on the order of seconds to milliseconds such as monitoring the uptake of targeted contrast agents or investigating physiological responses to external stimuli as in functional brain imaging.

To date only a few real-time systems have been reported, all based upon linear arrays predominantly optimized for clinical imaging [8–12] although a few have been used for small animal experiments [2,13,14]. Due to the limited aperture of linear array transducers, features with high aspect ratio or orientations oblique to the transducer surface suffer distortion and azimuthal resolution is reduced. Tomographic systems, by offering complete angular views of the imaging target, overcome these limitations and provide both high resolution and accurate feature definition regardless of shape or location. Because of the large measurement surface, however, tomographic imaging has traditionally been demonstrated using mechanically scanned single or linear transducers. The long imaging times (minutes to hours) for these approaches have restricted applications to static or slowly varying phenomena.

We previously reported a 128-channel photoacoustic imaging system optimized for small animal imaging [15]. The system featured a curved ultrasound array that captured a 90-degree field of view in less than one second, but required sample rotation for complete tomographic imaging. The increased scan time (15-30 seconds) and registration errors associated with the mechanical rotation prevented imaging of short-duration physiological responses and introduced some distortion of the high-resolution (< 200 μm) images.

In this paper, we present results from a second-generation system employing a 512-element full-ring configuration [16]. By eliminating the speed and registration issues due to mechanical scanning and increasing the parallel receiver electronics, the system achieves, for the first time, a complete two-dimensional tomographic imaging in less than one second. The organization of this paper is as follows. We first present details of the system design and detailed characterization results of the system performance in terms of resolution and imaging volume. The capabilities of the system are then explored through *ex vivo* and *in vivo* imaging of mouse brain vasculature at up to 8 tomographic frames/second.

#109657 - $15.00 USD Received 3 Apr 2009; revised 17 May 2009; accepted 18 May 2009; published 8 Jun 2009
(C) 2009 OSA

2. Photoacoustic imaging system

Figure 1 depicts the experimental set-up and architecture of our 512-element, 360-degree photoacoustic tomography imaging system. A Ti:Sapphire (Symphotics TII, LS-2134) laser optically pumped with a Q-switched Nd:YAG laser (Symphotics-TII, LS-2122) delivers 8-12 ns pulses at 15 Hz with wavelength tunable from 700 to 950 nm. The beam is expanded with a Galilean telescope assembly and subsequently diverged with either a plano-concave lens or homogenized by a circular profile engineered diffuser (ED1-S20, ThorLabs, Newton, NJ). The laser beam is positioned at the center of the transducer and strikes the stage orthogonal to the imaging plane of the transducer for maximum uniformity.

The transducer array, custom manufactured by Imasonic (Besancon, France), consists of 512 elements in a curved aperture such that they form a complete circle (i.e. 360 degrees), with a radius of curvature equal to 25 millimeters. The transducer array has a center frequency of 5 MHz and a bandwidth greater than 80%. The 1-3-piezocomposite elements are spaced with a lateral pitch of 0.3 mm; the maximum nearest neighbor acoustic crosstalk was measured to be −45 dB. Each element is directly shaped in elevation to produce a mechanical focal depth of 19 mm without the loss and acoustic aberrations of external lenses. The combined focal points of all elements form a ring around the central imaging region with a diameter of 1.2 cm. Within the elevation focal plane, phased array electronic scanning is used for focusing. Measurements of the sensitivity of individual elements with both pulse-echo ultrasound from a central stainless steel post and the photoacoustic signal from the transducer surface indicate a sensitivity variation of up to 12 dB across the entire array.

Due to the large number of channels, we have constructed our own front-end electronics and data acquisition system to obtain radio frequency (RF) data for tomographic image reconstruction. The laser Q-switch provides the master timing and triggers the acquisition system. Front-end receiver electronics reside on sixty-four boards, each serving eight channels. Further details of the board designs have been detailed in [15]. Upon absorption of the laser pulse, 512 dedicated low-noise, 20dB gain preamplifiers amplify the transient photoacoustic waves measured around the sample. To reduce the number of acquisition channels, multiplexers on each receiver board select one of eight channels and forward the outputs to low-noise second-stage amplifiers. The gain of the second stage amplifiers can be electronically controlled from 20 dB to 100 dB. The 64 output signals are filtered by 15 MHz anti-aliasing bandpass filters and sampled by parallel 40 MHz A/D channels with 10 bits precision. After each 64-channel acquisition, the computer outputs a pulse to advance the multiplexer setting and prepare for the next capture on the subsequent laser trigger. The data from each acquisition is DMA-transferred to RAM and accumulated over the experimental duration to maximize the imaging speed. The acquisition computer subsequently transfers the measurement data to disk for post-processing.

With the 8:1 multiplexing, eight laser firings are required to generate a complete 512-element capture. Data setup and transfer for results of a single acquisition can be performed at up to 8 Hz, leading to a maximum full-capture rate of 1 frame/second. As each tomographic image involves data over 8 distinct time instants, all frames actually reflect a time-averaged response over the acquisitions required for a complete data set. Using “sliding-window” data accumulation, where signals from each element with the nearest acquired time instant are retained for imaging, continuously updated time-averaged images can be achieved for each acquisition, leading to a higher rate of 8 frames/sec.

#109657 - $15.00 USD Received 3 Apr 2009; revised 17 May 2009; accepted 18 May 2009; published 8 Jun 2009
(C) 2009 OSA

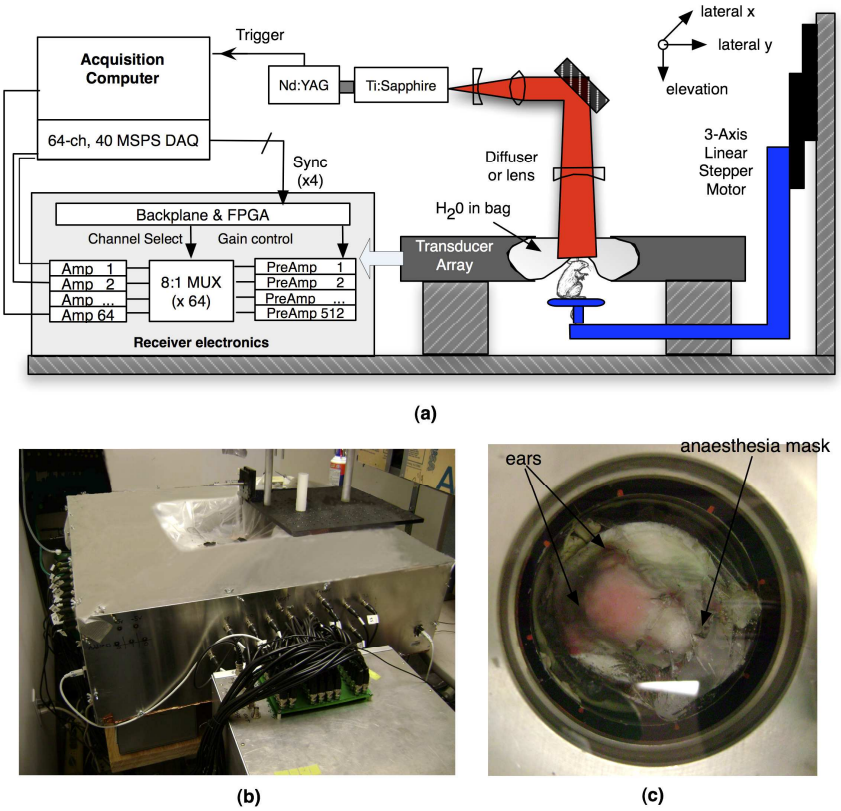

Fig. 1. Diagram (a) and photograph (b) of ring photoacoustic system. Photograph (c) of mouse within 50 mm transducer aperture.

3. Performance characterization

Resolution and the three-dimensional field-of-view are critical performance metrics for small-animal tomographic imaging systems. In order to assess the conformance to design, system characteristics were evaluated using both theoretical models and computer simulations and compared with experimental measurements. Simulation of the photoacoustic response was performed using the Field II ultrasound simulator [17]. As described in more detail in [18], the transducer element responses were calculated for thin cylindrical collections of spherical sources (emulating a 1.5mm long, 80 micron diameter source with long direction in elevation). The computed signals were then processed with a backprojection algorithm [19]. Due to the symmetry of the transducer, sources were located along a single radial line from the center to a radius of 18 mm. The resolution was calculated from the full-width half-maximum widths in the radial and transverse directions. In addition, the peak value of the imaged source was plotted for determination of the radial sensitivity arising from the fixed elevation focus.

Xu and Wang [20] derived the theoretical resolution for tomographic photoacoustic systems without acoustic focusing. The results for a cylindrical measurement surface predict a nearly constant radial resolution with a linearly increasing transverse resolution ranging from zero at the center to the width of each transducer element at the periphery. As the contributions from individual elements are weighted by the location of the source relative to the elevation focus, the resolution can degrade more rapidly than for unfocused systems due to fewer effective numbers of elements contributing to the image. In the calculations, both the spatial and bandwidth contributions to the resolution were considered.

#109657 - $15.00 USD Received 3 Apr 2009; revised 17 May 2009; accepted 18 May 2009; published 8 Jun 2009
(C) 2009 OSA

Experimentally, the resolution and spatial response was evaluated using a short section (< 2 mm) of 80-micron diameter black thread mounted on a plastic fiber. The thread was scanned radially in 0.5 mm increments. To minimize illumination variations, a diffuser was used to homogenize the light to a diameter larger than the ring. Figure 2 (a) shows the measured and calculated resolutions to a radius of 18 mm. The radial resolutions agree well with a nearly constant value throughout the range of distances. The lateral resolution follows the theoretical curve well to a radius of about 10-12 mm beyond which non-linear decreases in resolution are observed due to the defocusing of more distant elements.

Figure 2 (b) compares the measured and simulated spatial response along a radial line. The response peaks at the radial distance corresponding to the fixed elevation focus and drops by less than 3 dB throughout the central region. Defining the imaging field-of-view by a response within 6 dB of the peak, the system provides an imaging domain of approximately 2 cm diameter. Within this region, the resolution is better than 300 microns. To provide a more realistic view of the three-dimensional response surface, Fig. 2(c) depicts the simulated response through a cross-sectional cut dividing the transducer into two identical halves. The plot illustrates that the imaging "plane" consists of a disk of 2 cm diameter with thickness ranging from 600 microns at the elevation focus to 2 mm at the center. This slice thickness and diameter enables tomography for an entire small animal brain or anatomical region with selectivity to discriminate depth-dependent vascularization.

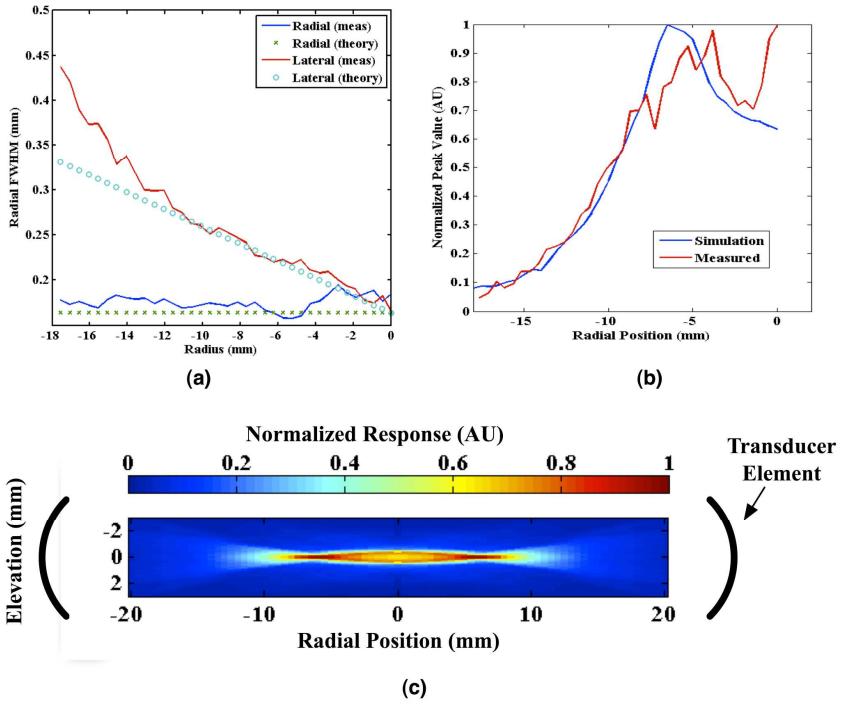

Fig. 2. (a) Measured and theoretical resolution versus distance from the center of the transducer. (b) Measured and simulated response vs. distance from the transducer center. (c) Simulated cross-sectional view of spatial response with location for a radial cut dividing the transducer into two halves. The locations of the transducer elements capping the ends of the region are indicated for reference.

4. Mouse/rat brain imaging

The brains of mice and rats were imaged to demonstrate the ability of the system to resolve vascular features and provide depth-resolved feature definition. *Ex vivo* experiments were

#109657 - $15.00 USD Received 3 Apr 2009; revised 17 May 2009; accepted 18 May 2009; published 8 Jun 2009
(C) 2009 OSA

performed with freshly sacrificed 50 g white rats with intact skull and skin (hair removed). The rats were acquired from the University of Connecticut Office of Animal Research and were euthanized in accordance with procedures of the University Institutional Animal Care and Use Committee as well as the National Institutes of Health. The rats were mounted in a 1.5" diameter PVC pipe with the skull level with the imaging plane. Full tomographic images were obtained at depths spanning over 6 mm with a 100-micron spacing. The incident fluence levels were maintained below 15 mJ/cm^2 with a wavelength of 750 nm.

Figure 3 presents images at depths corresponding to approximately 1 and 5 mm below the top of the skull along with open-skull photograph from dorsal and basal surfaces. Image reconstruction was performed using a backprojection algorithm after Wiener deconvolution of the transducer impulse response from the raw data using the measured noise spectrum at 60 dB electronic gain. At the dorsal plane, the superior sagittal and cerebral veins including branches are visible in addition to the top surfaces of the eyes. At the deeper cross-section, basalar veins and the middle cerebral artery can be observed along with ringed features near the brain stalk not visible in the photographs.

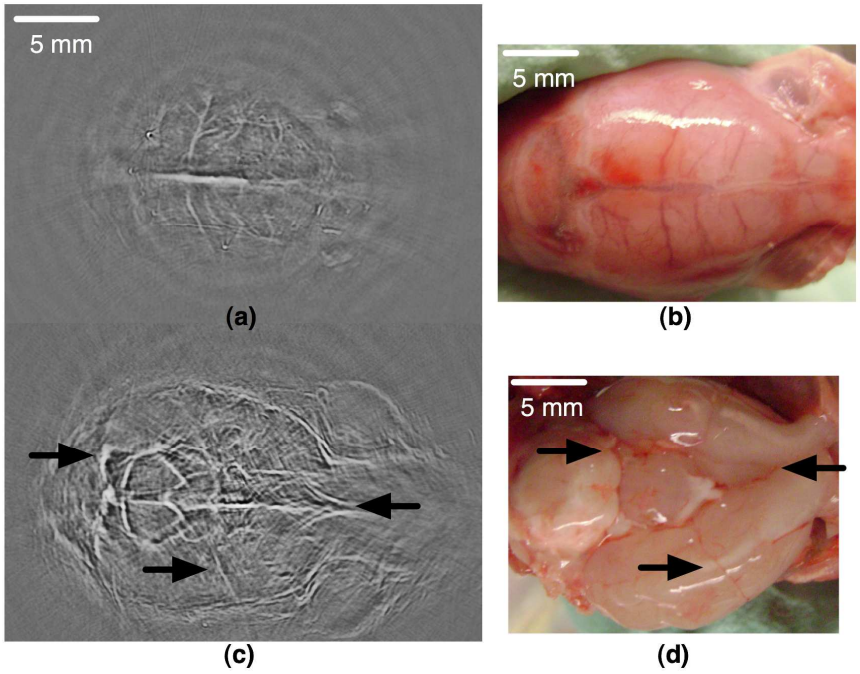

Fig. 3. *Ex vivo* images of rat brain at two depths spanning 4 mm. Image (a) and photograph (b) of surface vascularization. (c) Image at 4 mm below (a). Note the larger size of the brain at this level and the orbits of the eyes. (d) Photograph of basal surface annotated with features visible in photoacoustic image (c).

Figure 4 presents sectional images of an *ex vivo* 20 g white CD-1 mouse brain vasculature over a depth range of 4.5 mm. The cross-sections illustrate the capability of the system to provide volumetric imaging with an elevational resolution of 0.6 to 2 mm as illustrated by the presence of the largest vessels in about two layers.

#109657 - $15.00 USD Received 3 Apr 2009; revised 17 May 2009; accepted 18 May 2009; published 8 Jun 2009
(C) 2009 OSA

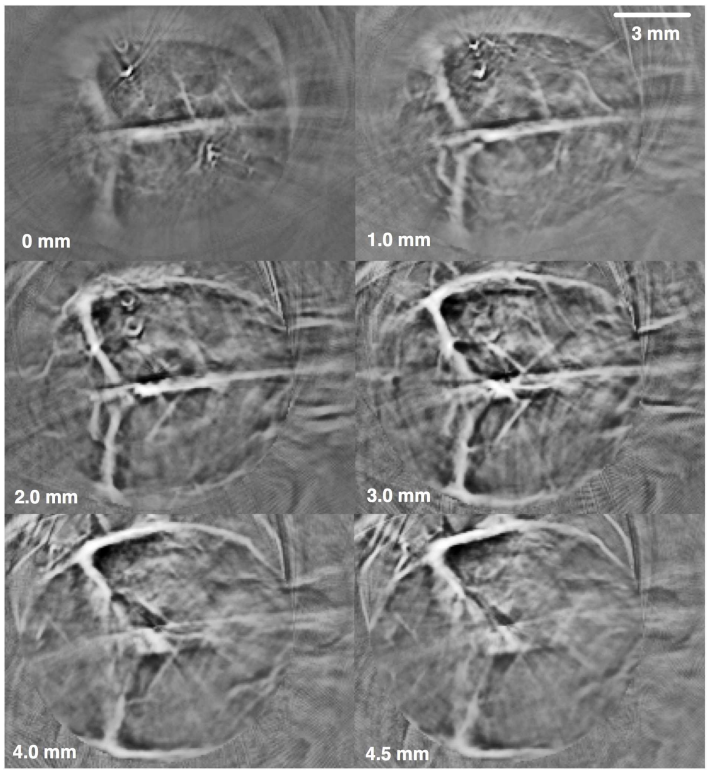

Fig. 4. Cross-sectional images of mouse brain vasculature at various depths.

In vivo imaging performance was evaluated using 4-6 week old female, CD-1 mice with masses of approximately 20 g. All experiments were carried out under a protocol approved by the University of Connecticut Institutional Animal Care and Use Committee. The mice were mounted upright in white PVC tubing with the skull level to the lateral imaging planes. An isoflurane (2%) gas system (VetEquip, Pleasonton, CA) delivered anesthesia through a custom miniaturized polyethylene mask to fit within the 44 mm aperture of the transducer. A thin heating pad, wrapped around the PVC tube, maintained a temperature of 37 °C and the blood oxygenation was monitored with a pulse oximeter. Because the imaging plane is 25 mm above the bottom plate of the transducer, a thin transparent plastic bag was mounted on the base and the mouse inserted into the transducer chamber under the bag with a thin layer of ultrasonic gel to provide acoustic coupling. The bag was fitted with sufficient slack to enable imaging at planes over a 1 cm range in depth. Prior to imaging, hair was removed using a depilitating cream.

Figure 5 presents photoacoustic images obtained from two mice with different head positioning. Because the imaging plane is a thin cylindrical volume, the observed feature definition in the brain can vary significantly with the orientation of the skull, particularly for cerebellum (steep slope) and anterior hemispheres (gentle slope). For a single cross-sectional image, tilting of the head can emphasize vasculature in the hemispheres (a) or cerebellum (b). Positioning is thus critical for real-time monitoring but less important for quasi-static volumetric imaging the animal where the animal is translated in the elevation direction. Interference from the breathing mask introduced reflections of the photoacoustic signals and limited the aperture angle to approximately 240 degrees. In combination with the extra loss from the plastic coupling bag, the mounting limitations reduced the visible features to the largest vessels as evident from comparison of Fig. 3 and Fig. 5. With further improvements in the setup imaging of smaller second order branches should be attainable.

#109657 - $15.00 USD Received 3 Apr 2009; revised 17 May 2009; accepted 18 May 2009; published 8 Jun 2009
(C) 2009 OSA

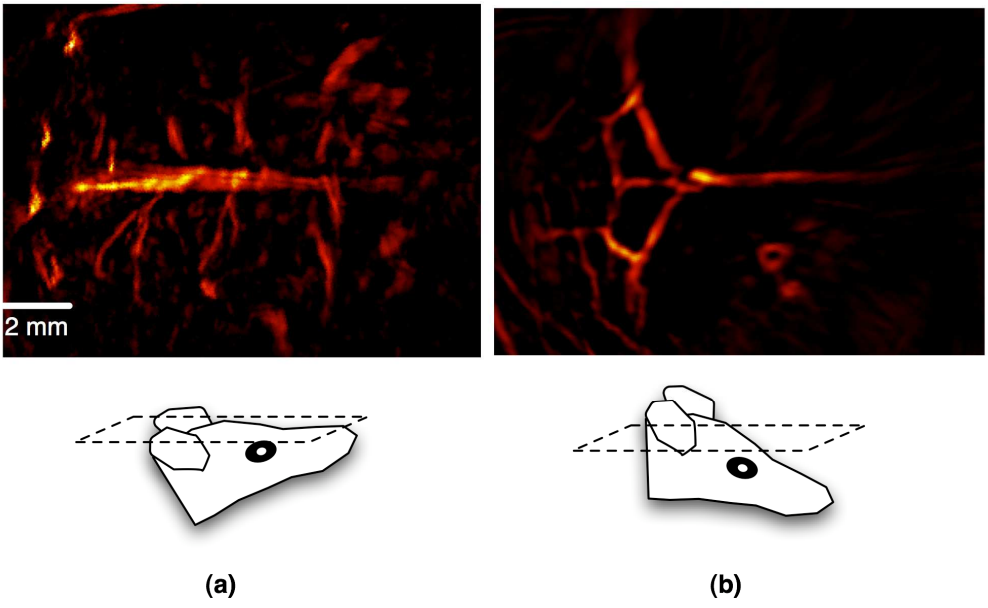

Fig. 5. *In vivo* photoacoustic images of brain vasculature for two mice with (a) dorsal and (b) ventral head tilt emphasizing hemispherical (a) and cerebellar vasculature (b).

5. Real-time imaging

With a capture rate of 8 frames/sec for a 64-channel subset and 1 frame/sec with a complete 512-element view, real-time tomographic imaging was demonstrated on both phantoms and mice in vivo. Figure 6 depicts frames from a 10-second sequence of dynamic ink flow through a 1 mm diameter polyethylene tube using a manual syringe push (movie online). To avoid partial view effects and maximize temporal resolution, a sliding window acquisition was adopted in which element data from the nearest (or equal) time instant were used for image formation. The images clearly track the flow through the tubing over the course of approximately 4 seconds with high spatial and temporal resolution possible only with tomographic methods.

#109657 - $15.00 USD Received 3 Apr 2009; revised 17 May 2009; accepted 18 May 2009; published 8 Jun 2009
(C) 2009 OSA

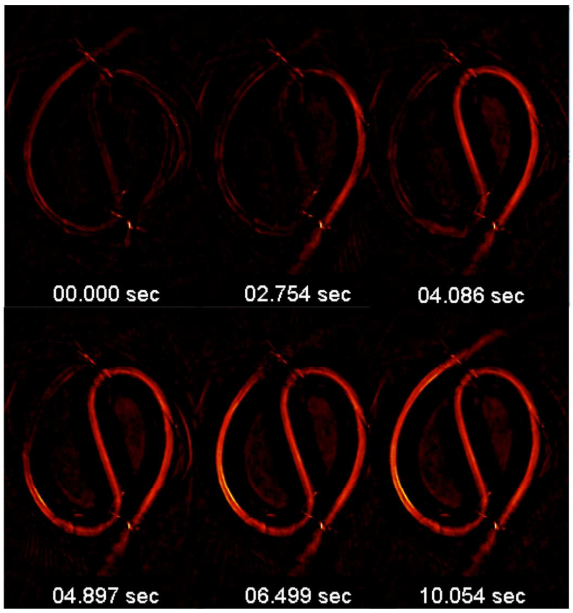

Fig. 6. Photoacoustic images of dynamic ink flow through a 1 mm diameter tube (Media 1).

As an illustration of the system performance at the borders of the imaging region, Fig. 7 depicts frames of an ink flow sequence through 580 micron (inner diameter) tubing over a three second interval. For this experiment, the two inner rings were filled with ink while ink was manually injected around the peripheral tube. Excellent definition of the tubing was maintained over the entire region of approximately 2 cm diameter. Results of other real-time measurements using this system and processed with limited-data algorithms for improved time resolution can be found in [21].

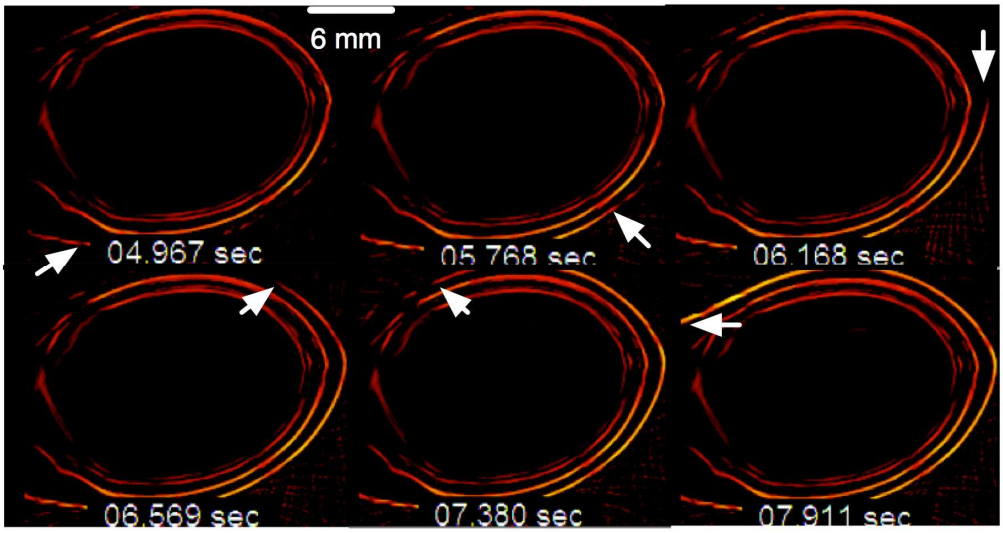

Fig. 7. Images of dynamic ink flow through 580 micron inner diameter tubing over a three second interval. The inner two tubes were held constant while ink was injected through the outer ring.

One important application of real-time systems is the potential for dynamic spectroscopic investigations that could monitor changes in oxygenation status both spatially and temporally.

#109657 - $15.00 USD Received 3 Apr 2009; revised 17 May 2009; accepted 18 May 2009; published 8 Jun 2009
(C) 2009 OSA

As a demonstration of the principle, the wavelength of the laser was manually scanned from approximately 700 nm to 900 nm during a 30-second *in vivo* imaging session with one of the mice shown in Section 4. Figure 8 depicts individual frames from the real-time sequence. The higher intensity for the 850 nm images is due to the increased penetration and higher absorption of the predominantly oxygenated hemoglobin. This experiment demonstrated the capability to perform wide-range, *in vivo* spectroscopic studies with sub-minute scan times.

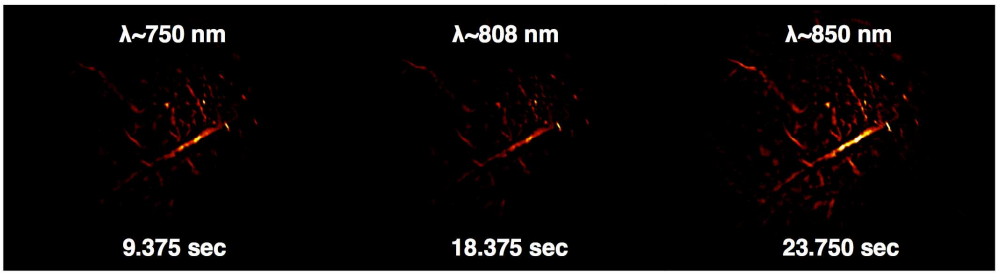

Fig. 8. Time-resolved imaging of mouse brain vasculature with fast wavelength scanning. The wavelength was swept from 710 nm to 900 nm over 30 seconds.

6. Discussion and conclusion

The system presented herein is the first capable of real-time tomographic photoacoustic imaging. The optimization of geometry and resolution for imaging of small animals provides a powerful platform for development and investigation of techniques for dynamic functional imaging. Speed constraints have thus far limited such studies to either quasi-static evaluation of responses to whisker stimulation [22], induction of hypo- and hyper-oxia [22], or uptake of contrast agents [23] or low spatial-resolution monitoring of oxygenation status [24]. Due to the 8:1 multiplexing, tomographic images from the system present an amalgamated view over a one-second interval. When combined with new algorithmic approaches for improving image quality with limited data sets, however, real-time sequences with temporal resolutions of less than 150 milliseconds have been achieved [21].

In conclusion, a 512-element tomographic system based upon a curved transducer array has been developed. With a resolution of better than 200 microns throughout an imaging volume of approximately 2 cm by 0.6 to 2.5 mm thick, the system provides complete 2D tomographic depth-resolved sections for three-dimensional small animal imaging. A 64-channel data acquisition, coupled with 8:1 multiplexing, enables real-time imaging with frame rates of 1 (full resolution) to 8 (partial view) frames/sec. The imaging performance was demonstrated through real-time imaging of dynamic fluid flow in phantoms and *in vivo* mouse brain vasculature imaging. The fast imaging capability offers the potential for complete two-dimensional *in vivo* small animal functional photoacoustic imaging studies at real-time rates.

Acknowledgement

We acknowledge the funding support from NIH (R01 NS46214) and The Donaghue Medical Research Foundation.

#109657 - $15.00 USD Received 3 Apr 2009; revised 17 May 2009; accepted 18 May 2009; published 8 Jun 2009
(C) 2009 OSA